Title: The Set Increment with Limited Views Encoding Ratio (SILVER) Method for Optimizing Radial Sampling of Dynamic MRI

Authors: S. Sophie Schauman[1], Thomas W. Okell[1], Mark Chiew[1]

[1] Wellcome Centre for Integrative Neuroimaging, FMRIB, Nuffield Department of Clinical Neurosciences, University of Oxford, Oxford, United Kingdom

Corresponding author contact details:
Sophie Schauman

FMRIB Centre
University of Oxford
Nuffield Department of Clinical Neurosciences
John Radcliffe Hospital
Headington
Oxford
OX3 9DU
United Kingdom

sophie.schauman@dtc.ox.ac.uk
Twitter: @sophieschau

Key words: radial trajectory, SNR optimization, dynamic MRI, golden ratio

Word count: 2800
Figure count: 5

Abstract

Purpose: To present and assess a method for choosing the increment between spokes in radially sampled MRI that can produce higher SNR than golden ratio derived methods.

Theory and Methods: Sampling uniformity determines image SNR when reconstructed using linear methods. Thus, for a radial trajectory, uniformly spaced sampling is ideal. However, uniform sampling lacks post-acquisition reconstruction flexibility, which is often needed in dynamic imaging. Golden ratio-based methods are often used for this purpose. The method presented here, Set Increment with Limited Views Encoding Ratio (SILVER), optimizes sampling uniformity when the number of spokes per frame is approximately known a-priori. With SILVER, an optimization algorithm finds the angular increment that provides the highest uniformity for a pre-defined set of reconstruction window sizes. The optimization cost function was based on an electrostatic model of uniformity. SILVER was tested over multiple sets and assessed in terms of uniformity, analytical g-factor, and SNR both in simulation and applied to dynamic arterial spin labeling angiograms in three healthy volunteers.

Results: All SILVER optimizations produced higher or equal uniformity than the golden ratio within the predefined sets. The SILVER method converged to the golden ratio for broad optimization sets. As hypothesized, the g-factors for SILVER were higher than for uniform sampling, but, on average, 26% lower than golden ratio. Image SNR followed the same trend both in simulation and in vivo.

Conclusion: SILVER is a simple addition to any sequence currently using golden ratio sampling and it has a small but measurable effect on sampling efficiency.

1. Introduction

Many recent MRI methods use radial k-space sampling instead of conventional Cartesian sampling. The benefits of radial sampling include reduced sensitivity to motion (1), and spatially incoherent aliasing when sampled below the Nyquist limit (2). For these reasons, radial sampling is often used in highly accelerated and/or dynamic imaging modalities.

Among radial sampling methods, uniformly distributed spokes are the most efficient in terms of signal-to-noise ratio (SNR) because SNR scales inversely with uniformity of sampling density (3). However, uniform radial sampling requires complete a-priori knowledge of how many k-space spokes will be combined to form an image in reconstruction. This is not always possible, for example, the number of spokes per frame is unknown at the time of acquisition when data is retrospectively binned based on respiratory or cardiac phases. Uniform sampling does also not allow for flexibility in reconstructing the same dataset at multiple temporal resolutions. Multiple temporal resolutions can be useful for retrospectively being able to trade spatial resolution for temporal resolution, as well as the ability to create a fully sampled temporal average image by combining data from many undersampled frames for example for coil sensitivity estimation (4).

A commonly used alternative to uniform sampling is the radial golden ratio (5) (GR), or tiny golden angle method (6). In these methods, the direction of each k-space sampling spoke is determined as a set angle increment from the previous spoke, such that each new spoke intersects the largest gap in k-space by the golden ratio. This results in relatively high uniformity for any number of subsequently acquired spokes and allows for complete flexibility in reconstruction.

However, because imaging experiments are generally designed for reconstruction with a specific temporal resolution or a range of window sizes (numbers of spokes per frame), the ability of GR sampled methods to get approximate uniformity for all possible window sizes is unnecessarily general for most applications. Therefore, we propose an alternative method, where optimization of the angular increment between subsequent spokes is performed for a restricted set of window sizes with the aim of maximizing the uniformity of sampling within that set. By relaxing the requirement for 'near-uniformity' to only apply to a specific set of window sizes, we hypothesize that higher sampling efficiency can be achieved whilst maintaining the favorable properties provided by the GR methods. In this paper we present a procedure for choosing a different fixed angular increment based on numerical optimization and compare our method with both the golden ratio method and with uniform sampling in simulations and in vivo. We call the proposed method the Set Increment with Limited Views Encoding Ratio (SILVER) method.

2. Theory

2.1. Properties of set increment sampling

A set increment for a 2D radial trajectory is simply a constant angle increment ($\theta = \alpha \times 180°$) from the previous spoke. How the data fills k-space depends on whether this step is a rational or irrational fraction of the whole circle.

When the step ratio, α, is a rational fraction, the exact same spoke will eventually be repeated, whereas if the step is irrational or rational with a very large denominator in its simplest form (practically irrational), no two spokes acquired within the duration of the experiment will be the same. In dynamic imaging experiments where the length of a frame is unknown a-priori, practically irrational increments are preferred to avoid acquiring the same spoke again within the frame. Similarly, if multiple temporal resolutions are required it is also beneficial to use irrational sampling to avoid duplicate spokes in the different window sizes, especially if data is combined across frames to be reconstructed such that the Nyquist criterion is met. For this reason, the golden ratio, which is often referred to as the most irrational number (7), is often used to sample when no periodicity is wanted, and every new spoke should fill k-space with near-optimal uniformity.

Another benefit of acquiring data in k-space with a set angular increment, regardless of whether the step ratio is rational or irrational, is that images with the same sampling efficiency can be reconstructed with any *N* subsequently acquired spokes. Each k-space trajectory will simply be a rotated version of the *N* previous spokes, rotated by $N\alpha \times 180°$ (Figure 1). This allows for sliding window (8) and view sharing (9) reconstructions with complete flexibility in where to start and end each frame.

Uniform radial sampling with full width spokes can be achieved with set increment sampling by choosing the angular increment between subsequently acquired spokes to be $\alpha_{uniform} = \frac{1}{N}$, where *N* is the number of spokes used to reconstruct one frame. In GR sampling, on the other hand, the step is instead approximately 111.24°, with $\alpha_{golden} = \frac{1}{\phi} = \frac{\sqrt{5}-1}{2} \approx 0.6180$. The aim of SILVER is to find a more optimal increment, $0 < \alpha < 1$, when near uniformity is only required for a certain set of window sizes.

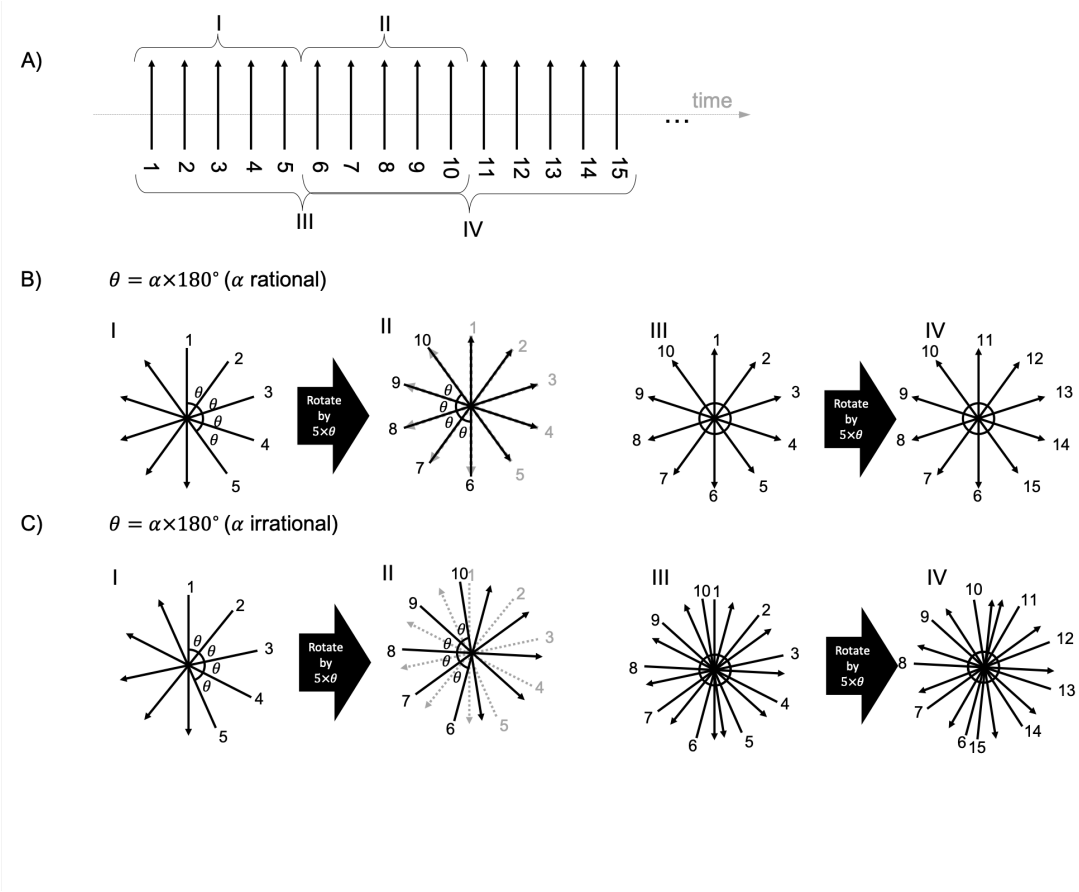

Figure 1 – The effect of set increment radial sampling with rational and irrational increments. (A) demonstrates four different groupings of subsequent spokes (I, II, III, and IV) and gives each spoke a number. (B) shows how the subsequent spokes in the different frames relate if α is rational (in this case 1/5), showing how both non-overlapping and overlapping frames have repeats of the same spokes. (C) shows the effect of an irrational α; Non-overlapping subsequent frames have no repeat spokes, and overlapping frames have some of the same spokes. In both (B) and (C) a subsequent frame (whether overlapping or not) is simply a rotaion of the previous frame and will thus have the same level of uniformity in each case.

2.2. Measuring sampling efficiency

Radial sampling in a linear acquisition and reconstruction framework has intrinsically lower SNR than Cartesian sampling due to the variable density with which k-space is sampled (10). Among radial sampling methods, radially uniform sampling achieves the highest SNR, and performance for a fixed number of spokes degrades the more non-uniform the sampling is.

Because SNR intrinsically depends on the local sampling density, different methods for estimating the local sampling density have been proposed. For radial sampling in particular, Winkelmann et al (5), defined sampling density by the inverse of the average azimuthal distance between adjacent spokes. Others have used analytically defined continuous density distributions that were used to generate the trajectory (10), numerically defined approaches using voronoi cells on spheres (11), or physical models based on electrostatic properties (12–14). Electrostatic methods are more commonly used as a 3D method but can also be generalized to 2D sampling. We used an electrostatic potential minimizing

model in SILVER because of its easy extension to 3D in the future and its high penalty for overlapping spokes.

The electrostatic potential method models the radial sampling pattern as an ensemble of unit charges placed on both ends of each spoke, constrained to the unit circle (or unit sphere in 3D). Efficiency compared to radially uniform sampling, η is then defined as the ratio of total electrostatic potential stored in the system of point charges, U, to a system with the same number of spokes in the lowest energy state (uniformly distributed spokes), U_{ref}

$$\eta = \frac{U_{ref}}{U} \tag{1}$$

with

$$U = \sum_{i,j=1}^{2N(i\neq j)} 1/r_{ij} \tag{2}$$

Where r_{ij} is the distance between the ith and jth points, and N is the number of spokes ($2N$ is therefore the number of spoke tips). For a set increment, α, U generalizes to a function of α and N. For a uniform distribution $\alpha = 1/N$ so U_{ref} is simply a function of N.

3. Methods

The SILVER method is an optimization problem, where the task is to maximize the minimum efficiency, η, for a pre-defined set of window sizes, $S = \{N_1, N_2, N_3, \ldots\}$. The objective function was therefore defined as:

$$\underset{\alpha}{\operatorname{argmax}}\left(\min_{N\in S}\left(\eta(\alpha, N)\right)\right) \tag{3}$$

with

$$\eta(\alpha,\ N) = \frac{U_{ref}(N)}{U(\alpha, N)} \tag{4}$$

Where N is the number of spokes in the window, and α is the set increment (as defined in section 2.1). To avoid local minima the optimization algorithm was restarted 100 times with 99 initial values of α drawn from a uniform probability distribution between 0 and 1 and one run with the golden ratio as the starting value. The optimization was performed in MATLAB R2018b (The MathWorks, Inc., Natick, Massachusetts, United States) using optimcon() in the Optimization Toolbox using the interior-point minimization algorithm.

SILVER was compared to GR sampling for a large range of plausible sets of window sizes, S. The efficiency of both methods was measured using the electrostatic potential method as described in section 2.2. First, continuous ranges of window sizes were explored. These sets contained a minimum window size of M spokes, and all intermediate window sizes up to a maximum window size, $M+R$, such that $S = \{M, M+1, \ldots, M+R\}$. M was set to 4, 16, and 32, and R was set from 1 to 100.

Similarly, the effect of optimizing for multiple specific temporal resolutions was examined. The efficiency for sets with $S = \{M, 2M\}$, and S = {M, $2M$, $3M$} were studied. Again, M was set to 4, 16, and 32. As a final case, where the GR approach is expected to perform optimally, we chose S to consist of Fibonacci numbers ($S = \{5,8,13,21,34\}$).

Maps of noise amplification due to acquisition operator non-orthogonality (g-factor (15)) were produced for SILVER, GR and uniform sampling trajectories. To create g-factor maps, the linear acquisition operator, $\boldsymbol{E = FS}$, with $\boldsymbol{S}$ being a set of eight coil sensitivities (compressed from a 32-channel sensitivity map measured in a phantom) and $\boldsymbol{F}$ being the discrete Fourier transform operator for samples along the trajectory, was calculated. The g-factor maps were then generated by analytic evaluation of the acquisition operator as described by Pruessmann et al. (15). g-factor maps were calculated for five different window sizes, $N = 16, 32, 48, 64, 128$. For each window size the map mean intensity was evaluated for a GR trajectory, a uniformly sampled radial trajectory, and for SILVER optimized for seven different sets of window sizes: $S = \{N, 2N\}$, $\{N, 2N, 3N\}$, $\{N\text{-}1, \ldots, N\text{+}1\}$, $\{N\text{-}2, \ldots, N\text{+}2\}$, $\{N\text{-}3, \ldots, N\text{+}3\}$, $\{N\text{-}4, \ldots, N\text{+}4\}$, $\{N\text{-}5, \ldots, N\text{+}5\}$.

Simulated multi-coil acquisition and reconstruction of a dynamic numerical phantom (a simple 64 x 64 moving image) was also done with the same coil sensitivities used for g-factor estimation. The image reconstruction quality of these iterative SENSE reconstructions was compared by measuring the spatial SNR (average signal in phantom divided by the standard deviation in the background) for 10 different noise instances.

Finally, in vivo dynamic pseudo-continuous arterial spin labeling angiography datasets were acquired from three healthy volunteers under a technical development protocol approved by local ethics and institutional committees using a 3 Tesla Verio scanner (Siemens Healthineers, Erlangen, Germany). Data was acquired with 5 different protocols:

1. Uniform sampling, 68 spokes per frame, 27 frames, $\alpha = 1/68$ (acceleration factor, R ≈ 4)
2. Uniform sampling, 153 spokes per frame, 12 frames, $\alpha = 1/153$ (R ≈ 2)
3. Uniform sampling, 306 spokes per frame, 6 frames, $\alpha = 1/306$ (R ≈ 1)
4. GR sampling, $\alpha = 1/\varphi \approx 0.6180\ldots$
5. SILVER optimized for $S = \{68, 153, 306\}$, $\alpha \approx 0.2770\ldots$

For all protocols, a 600ms labeling phase was followed by a 1288 ms continuous GRE Look-Locker readout (TE = 5.95 ms, TR = 11.7 ms, FA = 7º) where 108 spokes were acquired. A total of 1836 spokes (17 shots) were acquired for the tag and control conditions respectively. The spokes were

ordered such that combining the 17 shots resulted in the expected set increment trajectory (16). Total scan time for each protocol was 1 min 8 s.

All in vivo data was reconstructed with an iterative SENSE reconstruction in MATLAB. In vivo SNR was measured by applying a mask to the vessels and averaging for signal, the standard deviation in a wider mask excluding the vessels was considered noise. The masks are shown in Supporting Figure S1.

4. Results

Two examples of SILVER and GR theoretical efficiencies for specific window sizes are shown in Figure 2. The minimum efficiency of the SILVER trajectory within each targeted set was higher or equivalent to the trajectory produced by the GR method.

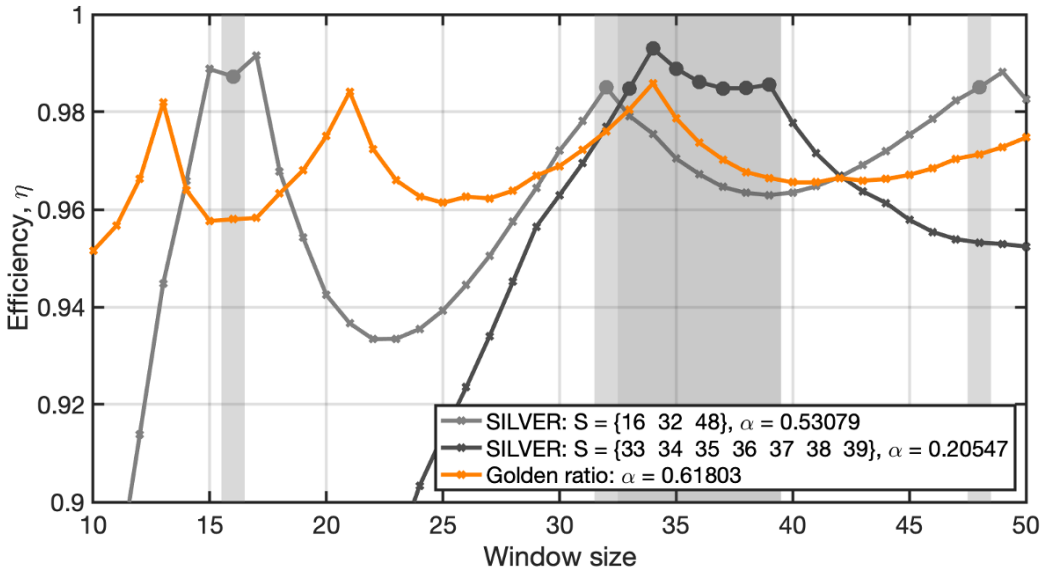

Figure 2 – Two examples of SILVER efficiencies (light and dark grey) compared with the golden ratio (orange) in a range of window sizes. The golden ratio has typical peaks at the Fibonacci numbers, SILVER has much more irregular peaks. The minimum efficiency for SILVER within the optimized range (shaded, round markers) is higher than for the golden ratio.

SILVER minimum efficiency was higher than the GR method for both continuous sets (Figure 3a), and multiple temporal resolutions (Figure 3b), although the improvement was negligible for large window ranges and for the set containing five Fibonacci numbers of spokes. The maximum observed improvement over GR was 4.7% (for $S = \{4, 5\}$). For a minimum window size, M, of 16 spokes the maximum efficiency increase was 3.8% (for $S = \{16, 17\}$), and remained above 1% for continuous sets with up to 10 members ($S = \{16, \ldots, 25\}$). Similarly, for a minimum window size, M, of 32, the maximum improvement was 2.2% (for $S = \{32,33\}$), and remained above 1% for continuous sets with up to 14 members ($S = \{32, \ldots, 45\}$). All multiple temporal resolution experiments except the set of

Fibonacci numbers had improvements of more than 1.8%, with the maximum improvement being 4.2% (for $S = \{4, 8\}$).

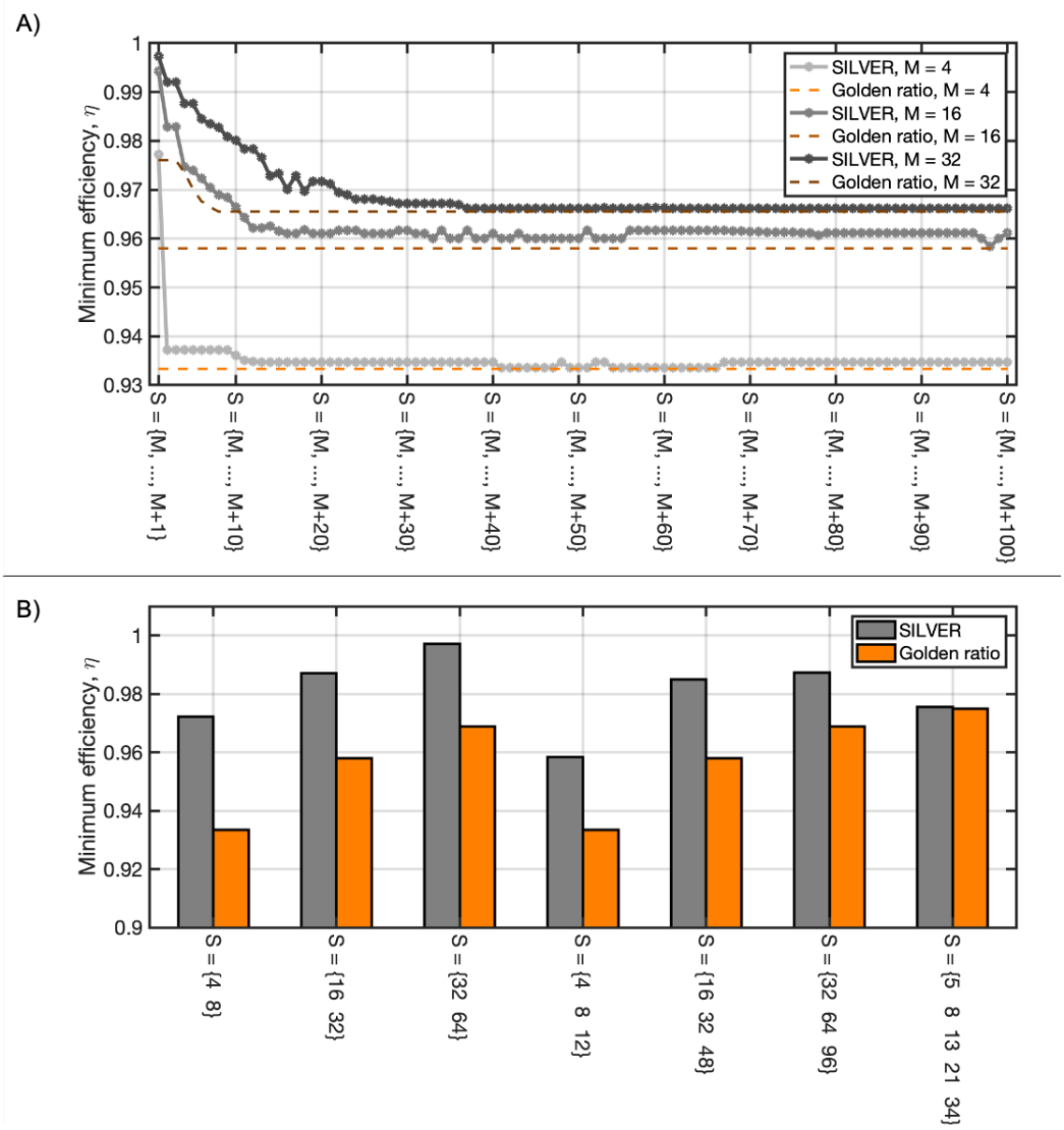

Figure 3 – For sets of continuous ranges of window sizes SILVER can outperform the golden ratio if the range is short enough. How short the range has to be depends on the minimum number of spokes as shown in (A). For pairs and triples of window sizes SILVER performed much better than the golden ratio, but in the golden ratio optimal case (Fibonacci numbers) they were equally good as shown in (B). The y-axis in both graphs, η, represents the minimum efficiency within the SILVER targeted range

The g-factor maps produced by the trialed SILVER trajectories had on average 10% higher g-factors than uniform sampling, but 26% lower than the GR method (the g-factors of GR were on average 49% higher than uniform). Figure 4a shows the result for the seven SILVER trials compared to uniform and GR. Figure 4b shows an example of relative g-factor maps for a SILVER and a GR trajectory for five different windows.

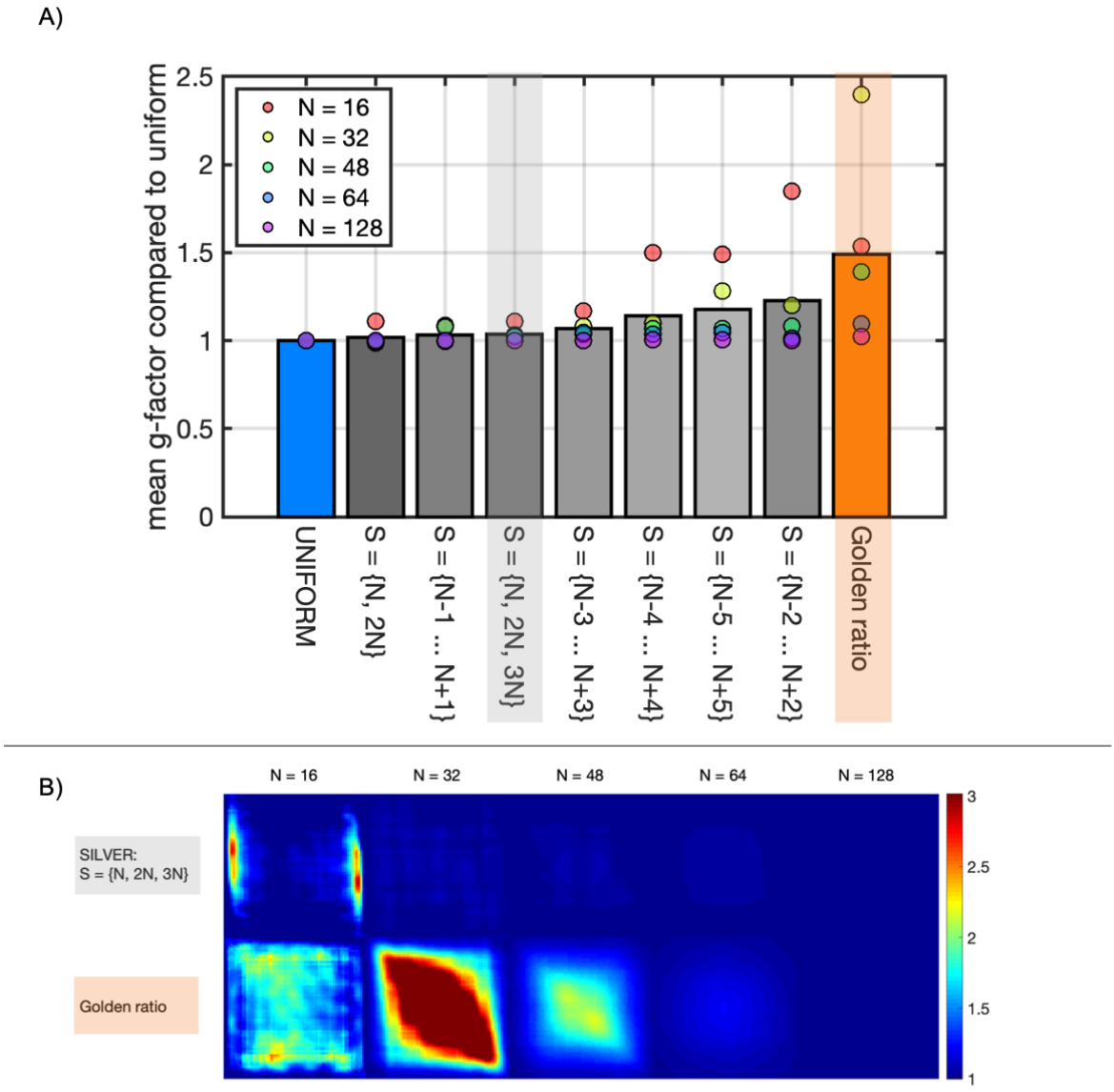

Figure 4 – Each bar in (A) shows the average relative g-factor across five window sizes. The bars are ordered lowest (uniform) to highest (golden ratio) with the seven different SILVER optimizations achieving intermediate g-factors. The colored circles show the results for each individual window size. A surprising result is that at 16 spokes the golden ratio has a lower mean g-factor than the worst SILVER result (red circles). Potential reasons to this are considered in the discussion section. Two of the columns in (A) are shaded, and the g-factor maps for each data point in the shaded columns displayed in (B). The golden ratio approach has especially high g-factors relative to uniform for a window size of 32 spokes. Both methods have low relative g-factors when the image is (close to) fully sampled at 64 or 128 spokes.

Figure 5a shows an example frame (32 spokes) of the reconstructions of the digital phantom and Figure 5b the temporal average of the in vivo angiograms (68 spokes/frame). In the phantom, noise amplification can clearly be seen in the SILVER and GR case compared to uniform sampling. SNR measurements (Figure 5c) for the 32 and 48 spoke case followed the expected trend of $SNR_{unifoirm} > SNR_{SILVER} > SNR_{Golden\_ratio}$. However, in the 16 spoke case, all three methods struggled with noise amplification and had low SNR. Surprisingly, in the 16 spoke case $SNR_{SILVER} > SNR_{Golden\_ratio} > SNR_{uniform}$. SNR measured across the three subjects (Figure 5d) follow the expected pattern. The reconstruction with uniform sampling exhibits streaking when averaged across frames because each

frame had the exact same trajectory and thus residual streaking artifacts add up. This is artefact is notably missing from both the SILVER and GR image.

Videos containing the dynamic images are available in Supporting Information Videos S1-S4.

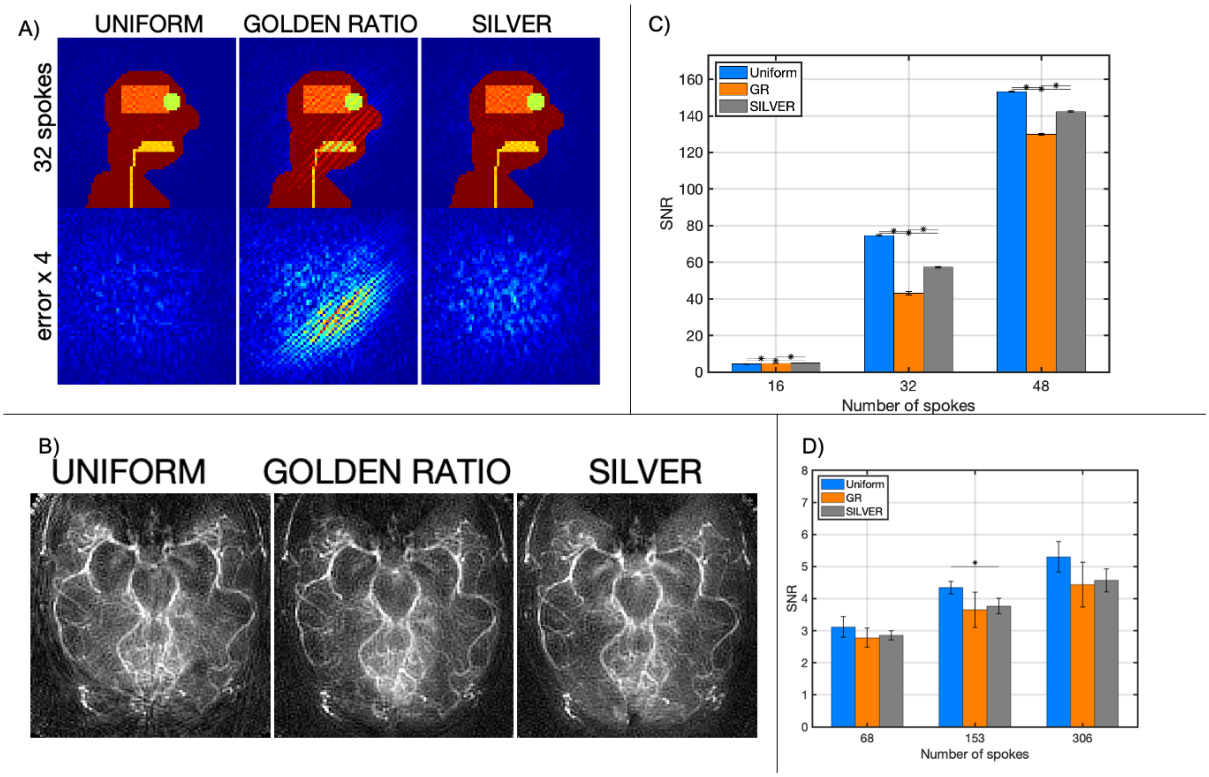

Figure 5 – (A) shows a frame of the dynamic phantom reconstructed with 16 spokes per frame with either a uniform radial, golden ratio, or SILVER trajectory. Below each image is the error between it and the ground truth. There are small but measurable SNR differences between these reconstructions as shown by the bar chart in (C). Similarly, an example of an in-vivo angiogram (temporal average after reconstruction) acquired with three different trajectories (68 spokes per frame) is shown in (B) and the combined SNR measurements in three subjects in (D). In vivo SNR has the same trend as the simulations although the differences are not significant.

5. Discussion and conclusions

We have presented a method of choosing an optimal angular increment for dynamic radial MRI when the set of window sizes to consider is constrained. We have showed that this method results in small but measurable and potentially valuable increases in SNR compared to the more general golden ratio method, with only a minor change required to the acquisition protocol. The SILVER framework also has a potential to be extended to imaging with other trajectories that have previously been derived from the golden ratio, e.g. spirals (17,18), cones (19), and even Cartesian sampling (20).

Because orthogonality of the acquisition operator depends on the coil sensitivities, as well as the sampling trajectory, optimizing for sampling uniformity alone does not always produce the optimal trajectory. When the undersampling factor is high, the orthogonality of the acquisition operator is

highly dependent on the combination of these two factors. This could explain why, at 16 spokes, the golden ratio performed better than one of the SILVER optimizations (Figure 4a) and why SNR in the phantom reconstructed with 16 spokes/frame did not strictly follow the expected trend based on uniformity alone. More orthogonal/uniform sampling also causes the recon operator to be better conditioned, which can reduce approximation errors of iterative linear reconstructions, which may explain the structured artefact in Figure 5a.

Without a-priori knowledge of coil sensitivity profiles, optimizing for uniformity is a tractable step towards optimized imaging. In future work, the SILVER framework could also be extended to optimize for properties other than trajectory uniformity through design of alternative cost functions, including cost functions that consider the incoherence of the operator for compressed sensing reconstructions (21). However, lower spatial coherence is achieved when there is no preferential direction of aliased energy, so radial uniformity alone should also be beneficial in compressed sensing reconstructions.

Both SILVER and the golden ratio method only optimize for subsequently sampled spokes, and there is no guarantee that binned data from multiple repeats of radial acquisitions are distributed optimally. Suggestions for overcoming this problem have been proposed for golden ratio sampling by e.g. Fyrdahl et al. (22), and this methods is equally applicable to SILVER.

In 3D, a set increment is harder to define than in 2D. Chan et al. (11) proposed the multi-dimensional golden means method, a 3D analogy of the golden ratio method with a constant azimuthal angle increment and a constant z-axis increment of the tip of the spoke constrained to the surface of a sphere. However, subsequent frames generated with this method are not simply a rotation of the spokes from the previous frame, and therefore not all image frames are guaranteed to have the same sampling efficiency. Because of the increased complexity of 3D radial sampling and the ambiguity of how to define a set increment, we constrained the scope of this paper to focus on the more commonly used 2D case, although extension of SILVER to 3D trajectories will be considered in future work.

In conclusion, SILVER is a method that generalizes set increment sampling beyond golden ratio derived methods when some knowledge of the number of spokes to combine in a frame is known a-priori. When SILVER is applied to a large set of window sizes whose uniformity cannot be improved upon, it simply returns the golden ratio (or a tiny golden ratio). Therefore, sometimes SILVER is better than gold, and when it is not, it is just as good.

6. Data availability statement

Code for SILVER optimization, all reconstructions, and analysis used in this paper are available on https://github.com/SophieSchau/SILVER. Anonymized data is available on https://zenodo.org/record/3904738.

7. Acknowledgements

This study was supported by funding from the Engineering and Physical Sciences Research Council (EPSRC) and Medical Research Council (MRC) (EP/L016052/1), the Royal Academy of Engineering (RF201617\16\23)(RF/132). The Wellcome Centre for Integrative Neuroimaging is supported by core funding from the Wellcome Trust (203139/Z/16/Z). T.O. is supported by a Sir Henry Dale Fellowship jointly funded by the Wellcome Trust and the Royal Society (220204/Z/20/Z).

8. References

1. Nishimura DG, Jackson JI, Pauly JM. On the nature and reduction of the displacement artifact in flow images. Magn. Reson. Med. 1991;22:481–492 doi: 10.1002/mrm.1910220255.

2. Lustig M, Donoho DL, Santos JM, Pauly JM. Compressed Sensing MRI. IEEE Signal Process. Mag. 2008;25:72–82 doi: 10.1109/MSP.2007.914728.

3. Liao J-R, Pauly JM, Brosnan TJ, Pelc NJ. Reduction of motion artifacts in cine MRI using variable-density spiral trajectories. Magn. Reson. Med. 1997;37:569–575 doi: 10.1002/mrm.1910370416.

4. Feng L, Grimm R, Block KT, et al. Golden-angle radial sparse parallel MRI: Combination of compressed sensing, parallel imaging, and golden-angle radial sampling for fast and flexible dynamic volumetric MRI. Magn. Reson. Med. 2014;72:707–717 doi: 10.1002/mrm.24980.

5. Winkelmann S, Schaeffter T, Koehler T, Eggers H, Doessel O. An Optimal Radial Profile Order Based on the Golden Ratio for Time-Resolved MRI. IEEE Trans. Med. Imaging 2007;26:68–76 doi: 10.1109/TMI.2006.885337.

6. Wundrak S, Paul J, Ulrici J, Hell E, Rasche V. A Small Surrogate for the Golden Angle in Time-Resolved Radial MRI Based on Generalized Fibonacci Sequences. IEEE Trans. Med. Imaging 2015;34:1262–1269 doi: 10.1109/TMI.2014.2382572.

7. Phillips T. The Most Irrational Number. American Mathematical Society Feature Column. http://www.ams.org/publicoutreach/feature-column/fcarc-irrational1. Published August 1999. Accessed June 3, 2020.

8. Jeong HJ, Cashen TA, Hurley MC, et al. Radial sliding-window magnetic resonance angiography (MRA) with highly-constrained projection reconstruction (HYPR). Magn. Reson. Med. 2009;61:1103–1113 doi: 10.1002/mrm.21888.

9. Zhou Z, Han F, Yu S, et al. Accelerated noncontrast-enhanced 4-dimensional intracranial MR angiography using golden-angle stack-of-stars trajectory and compressed sensing with magnitude subtraction. Magn. Reson. Med. 2018;79:867–878 doi: 10.1002/mrm.26747.

10. Tsai C-M, Nishimura DG. Reduced aliasing artifacts using variable-density k-space sampling trajectories. Magn. Reson. Med. 2000;43:452–458 doi: 10.1002/(SICI)1522-2594(200003)43:3<452::AID-MRM18>3.0.CO;2-B.

11. Chan RW, Ramsay EA, Cunningham CH, Plewes DB. Temporal stability of adaptive 3D radial MRI using multidimensional golden means. Magn. Reson. Med. 2009;61:354–363 doi: 10.1002/mrm.21837.

12. Saff EB, Kuijlaars ABJ. Distributing many points on a sphere. Math. Intell. 1997;19:5–11 doi: 10.1007/BF03024331.

13. Jansons KM, Alexander DC. Persistent angular structure: new insights from diffusion magnetic resonance imaging data. Inverse Probl. 2003;19:1031–1046 doi: 10.1088/0266-5611/19/5/303.

14. Koay CG. A simple scheme for generating nearly uniform distribution of antipodally symmetric points on the unit sphere. J. Comput. Sci. 2011;2:377–381 doi: 10.1016/j.jocs.2011.06.007.

15. Pruessmann KP, Weiger M, Scheidegger MB, Boesiger P. SENSE: Sensitivity Encoding for Fast MRI. 1999:11.

16. Song HK, Yan L, Smith RX, et al. Noncontrast enhanced four-dimensional dynamic MRA with golden angle radial acquisition and k-space weighted image contrast (KWIC) reconstruction. Magn. Reson. Med. 2014;72:1541–1551 doi: 10.1002/mrm.25057.

17. Kim Y-C, Narayanan SS, Nayak KS. Flexible retrospective selection of temporal resolution in real-time speech MRI using a golden-ratio spiral view order: Speech MRI using Golden-Ratio Spiral. Magn. Reson. Med. 2011;65:1365–1371 doi: 10.1002/mrm.22714.

18. Kowalik GT, Steeden JA, Atkinson D, Montalt-Tordera J, Mortensen KH, Muthurangu V. Golden ratio stack of spirals for flexible angiographic imaging: Proof of concept in congenital heart disease. Magn. Reson. Med. 2019;81:90–101 doi: 10.1002/mrm.27353.

19. Zucker EJ, Cheng JY, Haldipur A, Carl M, Vasanawala SS. Free-breathing pediatric chest MRI: Performance of self-navigated golden-angle ordered conical ultrashort echo time acquisition: Free-Breathing Pediatric UTE Chest MRI. J. Magn. Reson. Imaging 2018;47:200–209 doi: 10.1002/jmri.25776.

20. Li S, Zhu Y, Xie Y, Gao S. Dynamic magnetic resonance imaging method based on golden-ratio cartesian sampling and compressed sensing. PLOS ONE 2018;13:e0191569 doi: 10.1371/journal.pone.0191569.

21. Lustig M, Donoho D, Pauly JM. Sparse MRI: The application of compressed sensing for rapid MR imaging. Magn. Reson. Med. 2007;58:1182–1195 doi: 10.1002/mrm.21391.

22. Fyrdahl A, Ramos JG, Eriksson MJ, Caidahl K, Ugander M, Sigfridsson A. Sector-wise golden-angle phase contrast with high temporal resolution for evaluation of left ventricular diastolic dysfunction. Magn. Reson. Med. 2019:mrm.28018 doi: 10.1002/mrm.28018.